Energy 284 (2023) 128703

Contents lists available at ScienceDirect

Energy

journal homepage: www.elsevier.com/locate/energy

Performance of HZSM-5 agglomerated in a mesoporous matrix in the fuel production from ethylene at atmospheric pressure

Zuria Tabernilla *, Ainara Ateka, Javier Bilbao, Andrés T. Aguayo, Eva Epelde **

Department of Chemical Engineering, University of the Basque Country (UPV/EHU), P. O. Box 644, 48080, Bilbao, Spain

ARTICLE INFO

Handling Editor: X Ou

Keywords:
Oligomerization
Ethylene
HZSM-5 zeolite
Hierarchical structure
Fuels
Coke deactivation

ABSTRACT

Ethylene oligomerization into liquid fuels at slightly over atmospheric pressure has been studied due to its interest to valorize online the excess of ethylene in sustainable olefins production processes and to intensify the production of fuel from refinery secondary streams. Runs were carried out in a fixed-bed reactor under the following conditions: 1.5 bar; 275–375 °C; space time, 2.7–16.2 $g_{catalyst}$ h mol_C^{-1}; time on stream, 5 h. The catalyst was prepared by agglomerating a HZSM-5 zeolite (SiO_2/Al_2O_3 of 30) in a mesoporous matrix (γ-Al_2O_3/α-Al_2O_3). The hierarchical porous structure of the catalyst enables to reach a pseudo-steady state with a remarkable remnant activity after an initial deactivation period of 2–3 h. Temperature shows a relevant effect on ethylene conversion and product distribution, where a C_{5+} liquid fuel yield of 55% above 325 °C and 10.6 $g_{catalyst}$ h mol_C^{-1} is obtained. At 325 °C, gasoline yield is 60%, with high olefin content (49%), which decreases at higher temperature, due to an increase in aromatic and paraffin concentration. Soft and hard coke analysis reveal the role of the matrix to attenuate deactivation. Moreover, above 325 °C the cracking of hard coke precursors deposited in the zeolite micropores prevails respect to their formation.

1. Introduction

The availability of fuels (gasoline, jet fuel and/or diesel) is encountering several challenges due to the increase in the energy demand, the depletion of fossil hydrocarbons and the increasingly restrictive environmental legislations on emissions, with special attention to the reduction of CO_2 emissions to minimize the effects of climate change [1–3]. The oligomerization of light olefins had a strong boost with the Mobil Olefins to Gasoline and Distillate (MOGD) process in a historic situation of oil supply falling [4] and nowadays it is an attractive initiative to produce environmentally friendly synthetic fuels and to reduce CO_2 emissions. The most developed routes for the production of olefins from sustainable sources are the Methanol-to-Olefins (MTO) process, using SAPO-34 catalyst [5], and its alternative from dimethyl ether (DME) (DTO process), using HZSM-5 zeolite-based catalysts [6]. Moreover, the one-step synthesis of olefins from CO_2 receives a considerable attention due to its thermodynamic, economic and energy efficiency advantages over the two-step synthesis process [7,8]. This synthesis is performed by alternative routes either following the modified Fischer-Tropsch synthesis [9] or with methanol/DME as intermediates [10].

In the conventional industrial processes for light olefin oligomerization (e.g. Shell, Gulfene, SHOP and Ethyl), homogeneous catalysts modified by transition metals and/or organic solvents are used for the production of linear alpha olefins (LAOs), of interest as polyethylene comonomers, and widely used in the formulation of plasticizers, lubricants and detergents [11–13]. However, for the production of fuels, the utilization of a heterogeneous catalyst shows notable advantages, as it requires less severe operating conditions, no separation of catalysts and solvent is needed; and the catalyst can be regenerated [14,15]. Bifunctional catalysts of transition metals (mainly Ni) supported on zeolitic microporous (HZSM-5, Hβ, HY) and mesoporous (SBA-15, MCM-22, MCM-41, MCM-48) materials are the most studied for the oligomerization of light olefins [16–20]. Konincks et al. [21] proposed a mechanism for the oligomerization of ethylene on Ni/Hβ catalyst, by explaining the synergy between the activity of Ni metal sites (active for the oligomerization steps) and the acid sites of the zeolite (for the alkylation, isomerization and cracking reactions).

The oligomerization of ethylene at low pressure is a lower cost alternative of interest for the intensification of liquid fuels production in

* Corresponding author.
** Corresponding author.
E-mail addresses: zuria.tabernilla@ehu.eus (Z. Tabernilla), eva.epelde@ehu.eus (E. Epelde).

https://doi.org/10.1016/j.energy.2023.128703
Received 14 April 2023; Received in revised form 11 July 2023; Accepted 7 August 2023
Available online 8 August 2023

refinery units, such as fluid catalytic cracking (FCC) or delayed coking unit (DCU), where ethylene is diluted in the dry gas stream. The oligomerization of this stream avoids its burning off as fuel gas, because ethylene separation is not economically justified otherwise [22]. This is the goal of the Conversion of Olefins to Distillate (COD) process in the PetroSA Fischer-Tropsch unit, to valorize a tail gas stream with a reduced concentration of ethylene and propylene [23]. The oligomerization of ethylene at low pressure can also be operated in line with olefin production processes under low or atmospheric pressure, from methanol [24], bio-ethanol [25], bio-oil [26], and polyolefinic plastics [27], where ethylene is the main olefin obtained. The high density and acid strength of the acid sites of HZSM-5 zeolite (without the presence of Ni, which moderates its acidity [28]), are suitable for the valorization of ethylene via low-pressure oligomerization. However, ethylene oligomerization requires a higher temperature due to its lower reactivity in comparison to other olefins of higher molecular weight [29,30]. One drawback is the extent of other side reactions, in particular β-scission cracking, olefin condensation to aromatics and coke formation, according to the mechanism shown in Fig. 1 [31–33]. In this mechanism, the activation of the oligomerization steps corresponds to the Lewis acid sites of the zeolite (of moderate acid strength), while the Brønsted acid sites (strong sites) are responsible for cracking (β-scission) and hydrogen transfer (aromatization and condensation) reactions, with formation of aromatics and coke. Jin et al. [34] have deepened on the role of the zeolite acid sites by proposing a kinetic model based on the single-event concept, in which the activation of the individual reactions has also been associated to acid sites of different acid strength.

A relevant challenge in the oligomerization of ethylene on HZSM-5 zeolite-based catalysts is the control of deactivation, especially at low pressure. The origin of deactivation is the retention of oligomers within the zeolite crystal channels, giving way to their blockage [32,35]. Thus, strategies for the attenuation of deactivation, avoiding the total blockage of the pores, include decreasing the crystal size of HZSM-5 zeolite [31] and the generation of mesopores within the zeolite structure [36], among others. Konincks et al. [20] have analyzed the deactivation results obtained on Ni modified zeolites in ethylene oligomerization. They highlight that catalysts reach a pseudo-steady state after a period of partial pore blocking. It is noteworthy that the remaining catalyst activity depends on the catalyst properties and operating conditions, which hampers data collection as well as a separated analysis of oligomerization and deactivation kinetics.

Díaz et al. [37,38] have checked the advantages of using a hierarchical porous structure of the catalyst particle, by agglomerating the HZSM-5 zeolite in a mesoporous matrix of γ-Al_2O_3 in the oligomerization of 1-butene. The presence of the matrix favors the diffusion of the heavy oligomers, by reducing the blockage of the zeolite micropore mouths. It is remarkable that within the range of operating conditions studied (175–325 °C and 1.5–40 bar) the catalyst reached a pseudo-steady state for 10 h on stream giving way to a substantial and constant remnant activity [37]. Moreover, the agglomeration provides a high mechanical and hydrothermal strength to the particle, which is important for process scale-up (which may require the use of a fluidized bed reactor) and, for the regeneration stage, in which the coke is removed by using two successive steps: firstly, coke sweeping using an inert gas; and subsequently, by combustion of the remaining coke [38].

In this work, we have explored the performance of a HZSM-5 zeolite catalyst agglomerated in a mesoporous matrix of γ-Al_2O_3/α-Al_2O_3, using this original configuration in the oligomerization of ethylene at low pressure for fuel production, mainly gasoline free of heteroatoms. The energy requirement of this process is lower than that for high-pressure oligomerization and catalyst deactivation by coke is attenuated (a key condition for the viability of the process). The target goal is to determine the optimal reaction conditions (temperature and space time) by studying its effect on the selectivity and deactivation. Due to the relevance regarding applications, attention has been paid to the results within the pseudo-steady state of the catalyst (reached by the presence of the matrix in the catalyst). Thus, operating maps have been proposed to establish the optimal operating conditions for gasoline production at stable catalyst conditions. Furthermore, due to its importance on the results and to obtain a rational explanation of the effect of reaction conditions and the presence of the matrix on the deactivation of the catalyst, the amount and different types of coke responsible for catalyst deactivation have been analyzed in detail. The results improve the prospects of valorizing ethylene-containing secondary streams proceeding from different refinery units with respect to the conventional processes (performed at high pressure).

2. Experimental

2.1. Catalyst preparation and characterization

A HZSM-5 zeolite (Zeolyst International, CBV-3024 E, with a SiO_2/Al_2O_3 molar ratio of 30) based catalyst was used for this study. The catalyst was prepared by agglomerating the zeolite (50 wt%) with pseudoboehmite (Sasol Germany, 32 wt%) and a colloidal dispersion of α-alumina (Alfa Aesar, 18 wt%). This material content is suitable to confer both mechanical and hydrothermal resistance, as well as to improve the accessibility of the reactants to the zeolite and gain resistance against coke deactivation avoiding the blockage of the micropore mouths, as determined in different reactions with rapid coke deposition [38–40]. The catalyst particles were obtained by wet extrusion, which are dried at room temperature for 24 h, sieved to a particle size of 0.12–0.3 mm; and, finally, calcined at 575 °C for 2 h. Note that with this calcination stage, the pseudoboehmite is converted into γ-Al_2O_3.

The physical properties (BET surface area, micro- and mesopore volume and distribution) of both fresh zeolite and catalyst were determined by N_2 adsorption-desorption in a Micromeritics ASAP 2010.

The acidity of the catalyst was determined by a temperature-

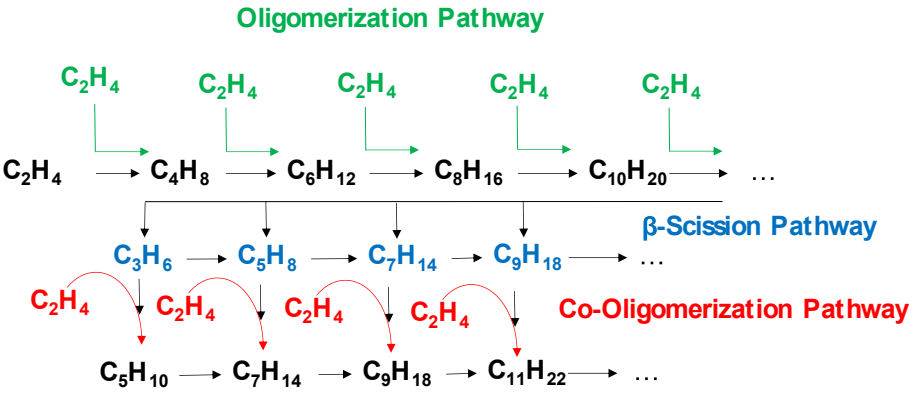

Fig. 1. Ethylene oligomerization reaction network on MFI zeolites. Adapted from Refs. [32,33].

programmed desorption of NH_3 (NH_3-TPD) in an Autochem 2920 Micromeritics equipment provided with a Harvard pump, a CS32 controller and connected on line to a Pfeiffer-Vacuum OmniStar mass spectrometer that allows the measurement of the adsorbed mass. Prior to analysis, the samples were swept with He (160 $cm^3\ min^{-1}$) at 550 °C. Then, the temperature was stabilized at 150 °C with a flow rate of He of 20 $cm^3\ min^{-1}$. At these conditions, the saturation of the sample was carried out by injection of NH_3 (50 $cm^3\ min^{-1}$). After the saturation of the sample, the physically adsorbed molecules were removed by He (20 $cm^3\ min^{-1}$) at 150 °C. Finally, a temperature-programmed desorption (TPD) was performed by heating up the sample up to 550 °C with a heating rate of 5 °C min^{-1} in a flow rate of He of 20 $cm^3\ min^{-1}$, recording at the same time the signal of NH_3.

In order to deepen in the identification of the type of acid sites in the samples (Brønsted and Lewis acid sites) pyridine adsorption was carried out at 150 °C using a Nicolet 6700 apparatus equipped with a Specac catalytic chamber. A tablet of ~10 mg of sample (zeolite or catalyst) was prepared by grinding and pressing the grains at 10–12 ton cm^{-2} for 15 min. The tablet was introduced in the catalytic chamber and was submitted to a heat pretreatment at 550 °C with a heating rate of 10 °C min^{-1}, under vacuum, to eliminate impurities. Then, temperature was cooled down at 150 °C and the signal was recorded with a frequency of 2 min^{-1}. The experimental procedure for these characterization techniques is well established in previous works [10]. The main physical and acid properties of zeolite and catalyst are summarized in Table S1 of the Supporting Information. The characterization of the matrix (γ-Al_2O_3/-α-Al_2O_3) has also been included for discussion.

The spent catalysts under the different reaction conditions studied (described in Section 2.2) were analyzed by using temperature-programmed sweeping with N_2 (N_2-TPS) followed by temperature-programmed oxidation (TPO) in a thermobalance TA Instruments Q5000, as follows [38]: (step 1) outgassing the sample (~15 mg) at 50 °C for 5 min with a flowrate of N_2 of 50 $cm^3\ min^{-1}$; (step 2) TPS, by sweeping at a heating rate of 10 °C min^{-1} in 50 $cm^3\ min^{-1}$ of N_2 up to 350 °C and kept for 20 min; (step 3) cooling down and stabilizing at 100 °C and switching the flow to air 50 $cm^3\ min^{-1}$ for 5 min; (step 4) TPO, by oxidation at a heating rate of 2 °C min^{-1} and stabilizing at 700 °C for 60 min; and (step 5) cooling down and stabilizing at 80 °C at a rate of 30 °C min^{-1} for 5 min. This combined technique allows quantifying the amount of confined oligomers (soft coke) and more developed coke species (hard coke) within the spent catalyst samples [38,41,42]. Note that prior to TPS-TPO analysis, the spent catalyst samples were swept in the reactor with 30 $cm^3\ min^{-1}$ of N_2 at the reaction temperature for 30 min to ensure the reproducibility of the analyses [38,43].

Additionally, transmission electron microscopy (TEM) images were obtained in a Phillips SuperTwin CM-200 microscope equipped with a LaB6 filament, using an accelerating voltage of 200 kV. Prior to the analysis, the samples were dispersed in ethanol, and subsequently, a drop of the suspension was deposited on a TEM copper sieve (300 Mesh) covered by carbon film for the analysis.

2.2. Reaction equipment and operating conditions

Ethylene oligomerization runs were carried out in a reaction equipment shown in Fig. S3 (and described in detail in Section S2) using a stainless steel fixed-bed reactor. The catalyst is mixed with inert carborundum (SiC) to ensure a constant height (1.5–2 cm) and isothermal conditions of the catalytic bed in all experiments. The following operating conditions were tested: 1.5 bar; 275–375 °C; space time, 2.7–10.7 $g_{catalyst}\ h\ mol_C^{-1}$, corresponding to catalyst mass between 0.25 and 1 g; ethylene (99%, Air Liquide) diluted with inert gas N_2 (20 vol%); and, time on stream (TOS), 5 h. The gaseous products (unconverted ethylene and non-condensed products, up to C_1–C_4 hydrocarbons), were analyzed online in a micro-gas chromatograph (Agilent 3000 A Micro GC). Gas product streams were analyzed every 4 min. Condensed liquid products (C_5–C_{20}), with insignificant contents of retained C_3 and C_4 compounds) were collected in periods of 15 min in the first hour on stream; 30 min in the second hour on stream; and every hour afterwards, in a cold trap at 2 °C, and *ex situ* analyzed by GC × GC/MS (Agilent 5975C Series GC/MSD). Example chromatograms are shown in Section S3. This equipment is a two-dimensional gas chromatograph coupled in-line with an XL MSD mass spectrometer equipped with a FID detector. GC × GC chromatograph is equipped with a non-polar column (DB-5MS, 30 m × 0.25 mm × 0.25 μm), and a polar column (HP-INNOWAX, 5 m × 0.25 mm × 0.15 μm), which enable the separation, identification and quantification of different hydrocarbon families (i.e. alkanes, cyclic alkanes, alkenes and aromatics) [44]. As an example, Fig. S4a shows the 3D view of a chromatogram obtained after primary and secondary separation in both non-polar and polar columns, while Fig. S4b shows the resulting contour plot for given reaction conditions. Note that the liquid products obtained are mainly paraffins, olefins and aromatics. Mass balance closed above 95 wt% for all the runs following the procedure described in Section S4.

The following main lumps were defined due to their commercial interest for the refinery and petrochemical industry: $C_3^=$ and $C_4^=$ olefins, C_{5+} fraction (including olefins, paraffins and aromatics). Additionally, the following lumped products were also defined based on their role within the reaction mechanism: $C_4^=$ (dimer) $C_6^=$ (trimer), $C_8^=$ (tetramer), $C_3^=$ and $C_{5\text{-}7}$ (paraffins and olefins) as cracking products, C_3 (propane) and C_4 (butanes) formed by hydrogen transfer reactions and BTX aromatics (A) and other aromatics (branched and double-ring, formed at high temperature). No methane has been formed under the operating conditions studied.

Given the interest of liquid products as fuel blends (gasoline, jet fuel and diesel), they were also analyzed by simulated distillation (ASTM D2887 Standard method), using an Agilent 6890 Series GC Systems gas chromatograph equipped with a semi-capillary column (DB-2887, 10 m × 0.53 mm × 0.88 μm) and a FID detector. The following cut points were established in accordance with the criteria used in the literature [41,45]: 50–150 °C, gasoline; 150–250 °C, jet fuel; and, >250 °C, diesel.

The results were evaluated in terms of conversion (X), yield (Y_i) and selectivity (S_i) of each lumped products, which are defined in Eqs. (1)–(3), respectively.

$$X = \frac{F_0 - F}{F_0} \cdot 100 \tag{1}$$

$$Y_i = \frac{F_i}{F_0} \cdot 100 \tag{2}$$

$$S_i = \frac{F_i}{F_0 - F} \cdot 100 \tag{3}$$

where F_0 and F, are the molar flowrate of ethylene in the feed and in the outlet stream, while F_i is the flowrate of *i* lump in the outlet stream. All terms are expressed in content C units.

3. Results

3.1. Effect of reaction temperature

3.1.1. Evolution of the yields of the main products with time on stream

Fig. 2 shows the evolution with time on stream of ethylene conversion (graph a) and the yield of main lumped products: $C_4^=$ (b), C_4 (c) and C_{5+} (d). More detailed information of other lumped product yields is depicted in Fig. S6.

Ethylene initial conversion sharply increases with temperature from 20% at 275 °C up to full conversion at 375 °C (Fig. 2a). At low-mild reaction temperature (275–350 °C) ethylene conversion notably decreases during the initial 1–2 h on stream, showing a sharp initial deactivation period. Subsequently, ethylene conversion slowly decreases or remains almost constant over time, reaching a pseudo-steady state at ~3 h on stream. This decrease in the conversion followed by the

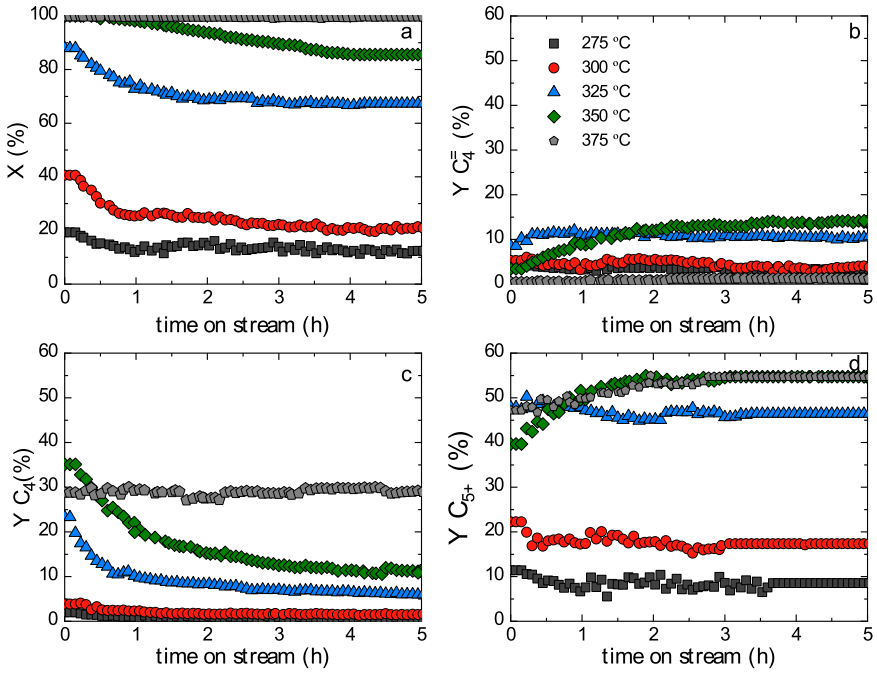

Fig. 2. Effect of temperature on the evolution with time on stream of: a) ethylene conversion; and the main product yields: b) $C_4^=$, c) C_4 and d) C_{5+}. Reaction conditions: 1.5 bar; W/F_0, 10.6 $g_{catalyst}$ h mol_C^{-1}.

pseudo-steady state has also been reported in prior works in the literature for light olefin oligomerization [37,46,47], and it is attributed to the partial pore blockage due to bulkier oligomers formed at low temperatures, which are retained in the catalyst matrix [40,46,48], even at low reactant conversion levels [32]. The presence of the mesoporous matrix contributes to reduce the blockage of the mouths of the zeolites micropores and to reach in a short time on stream a pseudo-steady state with remarkable remnant activity, as determined in different processes with fast coke deactivation [38–40,42]. Additionally, at the highest reaction temperature studied (375 °C), complete conversion of ethylene was obtained throughout 5 h on stream. This result is mainly attributable to the favoring effect of increasing temperature on the reaction rate, so that at 375 °C the catalyst is in excess, which explains that ethylene conversion is complete during 5 h on stream (Fig. 2a). Fernandes et al. [49] also showed similar trends in their study carried out at atmospheric pressure on an HZSM-5 zeolite catalyst, using space time values and temperature in the 4.2–18.7 $g_{catalyst}$ h $mol_{C2=}^{-1}$ and 300–500 °C ranges, respectively.

An increase in reaction temperature also leads to a significant variation in conversion, and distribution of the main lumped product yields. $C_{4=}$ yield is low (<2%) within the 275–300 °C range (Fig. 2b). At 325 °C, it shows an initial maximum value of 11%, which remains almost constant with time on stream, while at 350 °C this yield increases from 2% up to 14%, which remains constant after 2 h on stream. At 375 °C, $C_4^=$ yield is almost negligible. At the same time, C_4 yield sharply increases with temperature (Fig. 2c), especially above 325 °C, showing a maximum initial value of 30% at 375 °C, and remains almost constant with time on stream. At 325 and 350 °C, C_4 yield shows a fast deactivation rate during the first 2 h on stream. This suggests that during this initial period, secondary reactions of hydrogen transfer are favored because of the high acidity and acid strength of the fresh catalyst. However, the rate of these reactions decreases due to catalyst deactivation. After this deactivation period, within the pseudo-steady state of the catalyst, C_{5+} yield becomes dominant (Fig. 2d). C_5^+ yield at zero time on stream increases with temperature up to 325 °C and above this temperature the yield decreases since cracking reactions are favored with fresh catalyst. This situation changes with the deactivation of the catalyst (for these reactions and after the period of deactivation (pseudo-steady state)), C_{5+} yield reaches a maximum value of 55% at 350 °C and 375 °C. It should be noted that at 350 and 375 °C the presence of paraffins (Fig. 2e and Fig. S6f) and aromatics (mainly at 375 °C) (Fig. S6e) within C_{5+} fraction is high. This result indicates that the remnant activity of the catalyst is sufficient to maintain a high rate of aromatization and hydrogen transfer reactions at these temperatures [50].

3.1.2. Product distribution

Fig. 3 shows the effect of reaction temperature on the carbon number distribution within the different hydrocarbon families (olefins, paraffins and aromatics) when the pseudo-steady state of the catalyst is reached (at 3 h on stream). As observed, product distribution does not follow the Anderson-Schulz-Flory (ASF) distribution, where even carbon numbered hydrocarbons are exclusively formed as follows: $C_4 > C_6 > C_8$ … In fact, a remarkable formation of odd-numbered hydrocarbons stands out, which implies that these products do not directly result from oligomerization (true oligomerization pathway) reactions [51]. This fact confirms that apart from ethylene dimerization-trimerization and the oligomerization of butenes as reaction intermediates, other side reactions take place, by boosting the hetero-oligomerization pathways [52], as previously described in Fig. 1. At low temperature (275–300 °C) (Fig. 3a and b), the formation of olefins stands out, mainly $C_4^=$ and $C_5^=$. The formation of heavier olefins (C_8–C_{12}) starts to be significant at 300 °C. At intermediate temperature (325–350 °C) (Fig. 3c and d) olefins are the main products. However, some light paraffins (C_3–C_4) are also formed, while at 375 °C (Fig. 3e), the formation of light paraffins and aromatics (not considered in the scheme of Fig. 1) is greatly enhanced, which implies that the catalyst is active for secondary reactions of olefin conversion by hydrogen transfer and condensation during the pseudo-steady state. Hence, the aforementioned results reveal that within the 325–350 °C temperature range a compromise is reached between olefin and paraffins within the gasoline range since side reactions are limited.

3.1.3. Conversion and main product yield

The effect of temperature on ethylene conversion and on the yield of

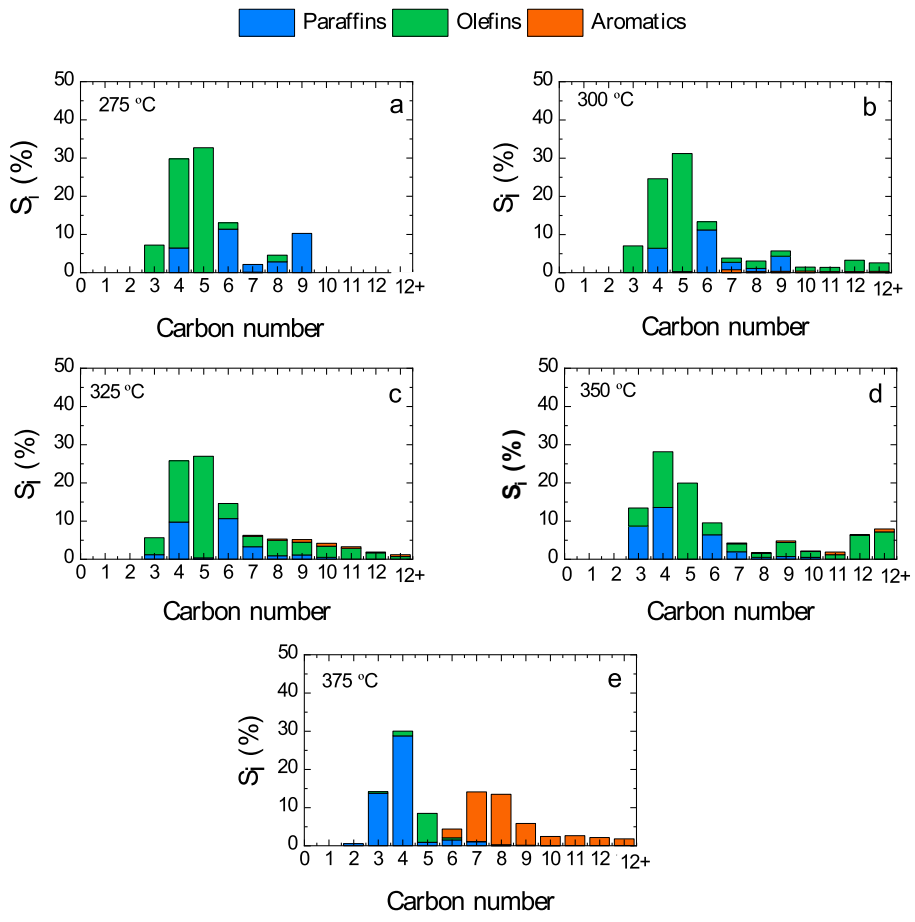

Fig. 3. Product distribution (selectivity) according to carbon number and family of hydrocarbons (paraffins, olefins and aromatics) at: a) 275 °C, b) 300 °C, c) 325 °C, d) 350 °C and d) 375 °C. Reaction conditions: 1.5 bar; space time, 10.6 $g_{catalyst}$ h mol_C^{-1}; 3 h on stream.

the main lumped products at the pseudo-steady state is shown in Fig. 4. Ethylene conversion increases sharply with temperature from 13.9% at 275 °C up to 99.6% at 375 °C. The low conversion obtained at 275 °C is in agreement with the results obtained by other authors [49,53] in kinetic tests carried out at atmospheric pressure. Fernandes et al. [49] obtained similar results in their parametric study on the conversion of ethylene to propylene and aromatics over an HZSM-5 zeolite catalyst. Likewise, Díaz et al. [37] established a minimum operating temperature of 225 °C at 1.5 bar, with a conversion of 10%, for 1-butene oligomerization over a HZSM-5 zeolite-based catalyst, under similar operating conditions (pressure and space time) to the ones used in this work. The higher reaction temperatures required for ethylene oligomerization are related to the lower stability of ethylene primary carbene ions in comparison to those of other olefins (propylene, butene) [34]. Zhou et al. [54] have demonstrated that at 450 °C the conversion of butene and propylene on SAPO-34 catalyst is 9 times faster than the conversion of ethylene. However, an increase in temperature leads to an increase in the reaction rate, and consequently, ethylene conversion increases and in turn, cracking reactions shown in Fig. 1 (of higher activation energy), are also favored [55]. A plausible operational solution would be to develop the oligomerization process in two steps [56]: initially, olefin mixtures with more than 50% ethylene content are oligomerized at 325–375 °C. Then, the oligomerization products are separated into C_{5+} liquid hydrocarbons, and C_3–C_4 gaseous alkenes. The latter are converted in a second step below 330 °C into gasoline and/or diesel fractions, reaching a high yield [56].

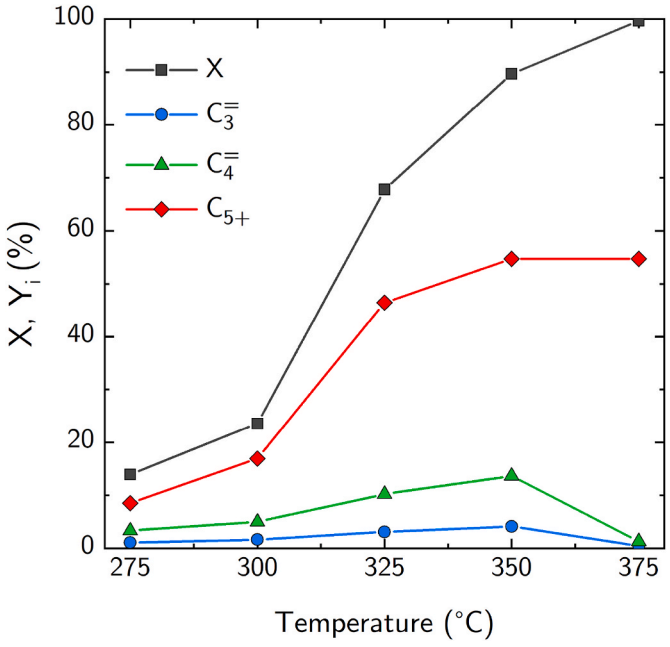

Fig. 4. Effect of the reaction temperature on ethylene conversion and yields of main lumped products. Reaction conditions: 1.5 bar; space time, 10.6 $g_{catalyst}$ h mol_C^{-1}; 3 h on stream.

As shown in Fig. 4 reaction temperature has also a great influence on the lumped product yield. Gasoline yield (C_{5+}) increases with temperature, from 8.6% at 275 °C up to 54.5% at 350–375 °C. A maximum in $C_3^=$ and $C_4^=$ yields is obtained at 350 °C, reaching values of 4.2% and 12.9% respectively. At 375 °C, propylene yield is almost negligible (1%),

but in turn, aromatic yield at this temperature is the maximum (40%) obtained for this study (Fig. S6g), which may be formed from propylene by condensation reactions [57].

3.1.4. Interest of liquid products as fuels

The liquid products have been analyzed by simulated distillation, as described in Section 2.2. The profiles (corresponding to the liquid product collected between 4 and 5 h on stream, pseudo-steady state) are shown in Fig. S7 for different reaction temperatures. It should be mentioned that at 275 °C no liquids have been obtained due to the low extent of ethylene conversion. Overall, as observed in Fig. S7, an increase in reaction temperature gives way to the formation of heavier hydrocarbons with higher boiling points. Thus, $T_{90\%}$ (temperature for 90% distilled volume) is greater from 264 °C to 297 °C when the reaction temperature increases from 325 °C to 375 °C.

To summarize the results of simulated distillation, Fig. 5 shows the effect of reaction temperature on the distribution (vol%) of the different fuels obtained: gasoline (distilled in the 50–150 °C range), jet fuel (150–250 °C), and diesel (>250 °C). Gasoline is the main fuel fraction obtained regardless reaction temperature, which peaks at 325 °C with a maximum value of 85.4 vol%. As previously mentioned, at low temperature, the oligomerization pathway is boosted, and, therefore, gasoline and jet fuel are the main fuel fractions. However, as temperature is raised diesel fraction is slightly favored, from 1.6 vol% at 350 °C up to 4.3 vol% at 375 °C.

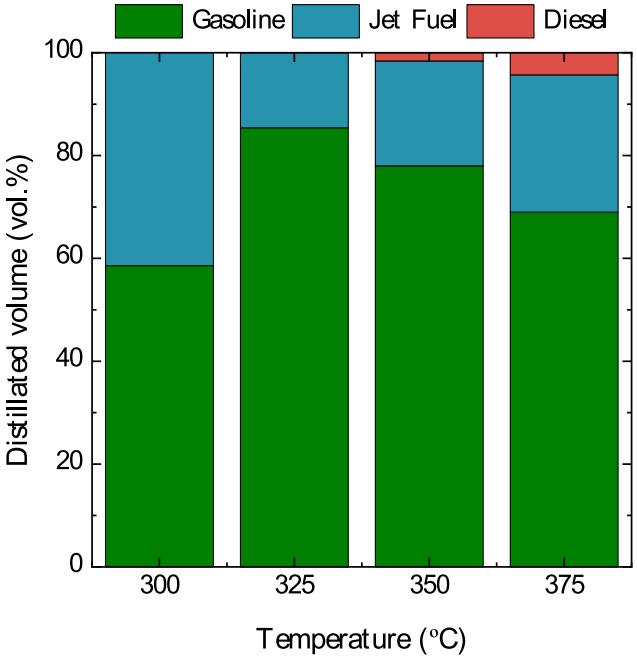

Fig. 5. Effect of the reaction temperature on the distribution of different type of fuels in the liquid product determined by the simulated distillation. Reaction conditions: 1.5 bar; space time, 10.6 $g_{catalyst}$ h mol_C^{-1}; 5 h on stream.

Additionally, C_{5+} fraction is mainly of olefinic nature (Fig. 3), except for 375 °C (Fig. 3d), where aromatics are dominant. Therefore, a mild hydrotreatment will be required to obtain a proper product stream to be added into refinery gasoline pools with high isoparaffin content, in order to achieve a high research octane number (RON). Furthermore, one of the main benefits of the fuel stream obtained via oligomerization is that it is free of S and N compounds, which results interesting for the refineries to meet the severe requirements of commercial fuels.

3.2. Effect of space time

3.2.1. Evolution of the main product yield with time on stream

Fig. 6 shows the effect of space time (W/F_0, ratio between catalyst mas and ethylene flow rate) on the evolution with time on stream of ethylene conversion (graph a) and on the yield of the main lumped products at 325 °C (graphs b-d). The conversion of ethylene at zero time on stream (Fig. 6a) increases as the space time increases, from an initial value of 50.8% for 2.7 $g_{catalyst}$ h mol_C^{-1} up to 100% for 16.2 $g_{catalyst}$ h mol_C^{-1}. As observed for the effect of temperature (Fig. 2), once again catalysts reach a pseudo-steady state after 2–3 h on stream. This effect was also observed by Mehdad and Lobo [58] in the conversion of ethane/ethylene mixture over Zn/ZSM-5 zeolites.

Higher space time values imply a larger number of active sites of the catalyst, by favoring the contact with ethylene and the extent of the reaction mechanism described in Fig. 1. This in turn influences the product distribution at zero time on stream (fresh catalysts), with a notable increase of C_4 yield (Fig. 6c). At the same time, C_{5+} yield (Fig. 6d) increases with space time, from 20% for 2.7 $g_{catalyst}$ h mol_C^{-1} to 55% for 16.2 $g_{catalyst}$ h mol_C^{-1}. Note that the formation of olefins is preferential at this temperature, where a low yield of $C_{5\text{-}7}$ paraffins is obtained, below 10% in all the cases studied (Fig. S8d). Moreover, the formation of aromatics is negligible (<5%) at 325 °C (Fig. S8e).

3.2.2. Product distribution

The effect of space time on the carbon number distribution of products (paraffins, olefins and aromatics) is shown in Fig. 7. As aforementioned, while studying the effect of reaction temperature (Fig. 3), the product distribution does not follow the ASF distribution, and the presence of odd carbon numbered hydrocarbons is notable, which implies that besides oligomerization, cracking and other side reactions take place in the reaction medium, according to the scheme shown in Fig. 1. At low space time values (Fig. 7a and b) olefins formation is dominant, especially butenes and pentenes, and to a lesser extent propylene and higher olefins ($C_{8\text{-}12}^{=}$). The formation of $C_3^{=}$ and $C_5^{=}$ is justified by the cracking of octenes formed by the oligomerization of butene after ethylene dimerization, or even by propylene itself, which reacts with ethylene to form olefins of 5 carbon atoms, or participates in further oligomerization to form higher olefins [59]. Similarly, the formation of propane and butane by hydrogen transfer reaction is also remarkable with increasing space time [60]. At high space time values (Fig. 7c and d), some aromatics begin to form, although their formation is limited under given reaction temperature (325 °C).

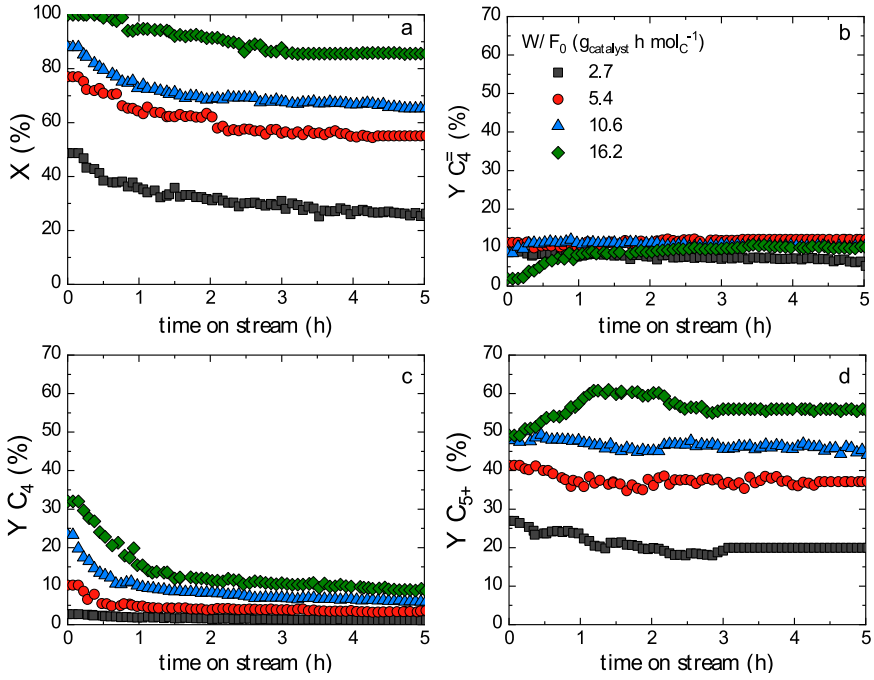

Fig. 6. Effect of space time on the evolution with time on stream of: a) ethylene conversion; and of the main product yields: b) $C_4^=$, c) C_4, and d) C_{5+}. Reaction conditions: 1.5 bar; 325 °C.

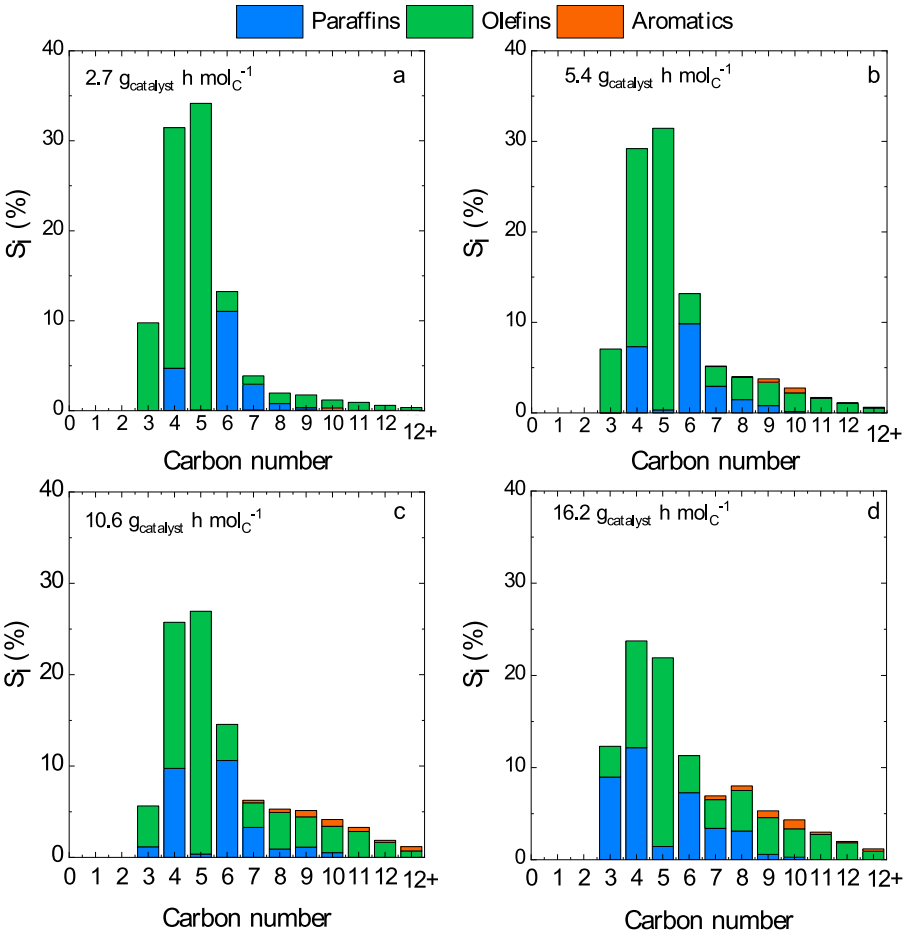

Fig. 7. Product distribution (selectivity) according to carbon number and family of hydrocarbons (paraffins, olefins and aromatics) for space time values of: a) 2.7 $g_{catalyst}$ h mol_C^{-1}, b) 5.4 $g_{catalyst}$ h mol_C^{-1}, c) 10.7 $g_{catalyst}$ h mol_C^{-1}, and d) 16.2 $g_{catalyst}$ h mol_C^{-1}. Reaction conditions: 1.5 bar; 325 °C; 3 h on stream.

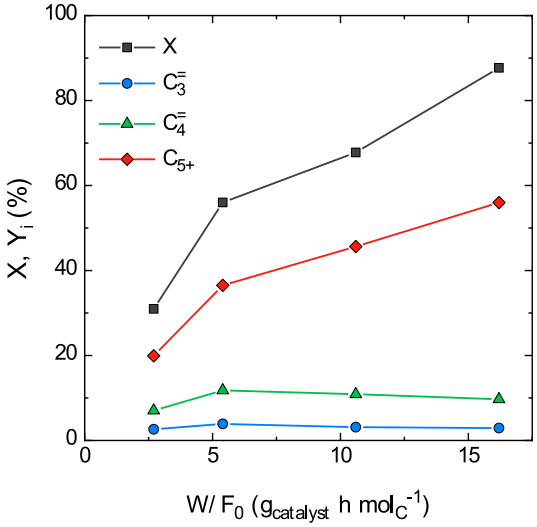

Fig. 8. Effect of space time (W/F_0) on ethylene conversion and on the main lumped product yield. Reaction conditions: 1.5 bar; 325 °C; 3 h on stream.

3.2.3. Conversion and main product yield

The effect of space time on ethylene conversion and on the yield of the main lumped products is shown in Fig. 8, corresponding to runs at 325 °C. Ethylene conversion increases progressively upon increasing space time, reaching a maximum value of 87.7% at 16.2 $g_{catalyst}$ h mol_C^{-1}. Moreover, the effect of space time provides a better understanding of the reaction mechanism. In this sense, light olefin ($C_3^=$ and $C_4^=$) yield decreases when increasing space time, being the decay more pronounced above 5.4 $g_{catalyst}$ h mol_C^{-1}. In contrast, C_{5+} yield increases with space time, reaching a maximum of ~57% at the highest space time value studied. The effect of space time on ethylene oligomerization on HZSM-5 catalysts has also been studied elsewhere [49,55], concluding that an increase in the contact time notably decreases the formation of dimers and trimers of ethylene, favoring the formation of secondary products such as light paraffins and aromatics. Silva et al. [61] also observed this effect in the oligomerization of 1-butene on a TUD-1 catalyst, in which an increase in the space time greatly decreased trimer formation, by favoring the formation of cracking products.

3.3. Reaction maps

The results obtained at different values of temperature and space time allow to determine the optimal combination of these conditions to maximize ethylene conversion or the yield of a given product fraction. In Fig. 9 the joint effect of temperature and space time on ethylene conversion (graph a), $C_4^=$ (b) and C_{5+} (c) yield is shown. Additionally, Fig. S9 shows these temperature-space time contour maps for the remaining lumped product yields ($C_3^=$, $C_6^=$, $C_8^=$, C_4, $C_{5\text{-}7}$ and aromatics). These maps were obtained by linear interpolation of the experimental data obtained at the pseudo-steady state (3 h on stream), using the *interp2* function of MATLAB [2].

As observed in Fig. 9a, high ethylene conversion levels (>92%) are attained at high temperature and space time values. Likewise, $C_4^=$ yield (Fig. 9b) is boosted for an intermediate temperature range (325–350 °C) and with relatively high space time values (10.6 $g_{catalyst}$ h mol_C^{-1}). On the other hand, the maximum gasoline yield, (C_{5+} fraction, Fig. 9c), ~60%, is attained working at temperatures above 325 °C and with space time values equal or higher than 16.2 $g_{catalyst}$ h mol_C^{-1}.

The formation of ethylene trimers ($C_6^=$, Fig. S9b) and tetramers ($C_8^=$, Fig. S9c) is favored at low temperature (275 °C) and high space time values, and so is propylene (Fig. S9a). However, C_4 (Fig. S9d) and $C_{5\text{-}7}$ (Fig. S9e) paraffin yield is greatly enhanced at high temperatures and high space time values (5.4 $g_{catalyst}$ h mol_C^{-1}), as hydrogen transfer reactions are favored to some extent. The formation of aromatics (Fig. S9f) is strongly influenced by temperature and a maximum value of ~40% is obtained at 375 °C.

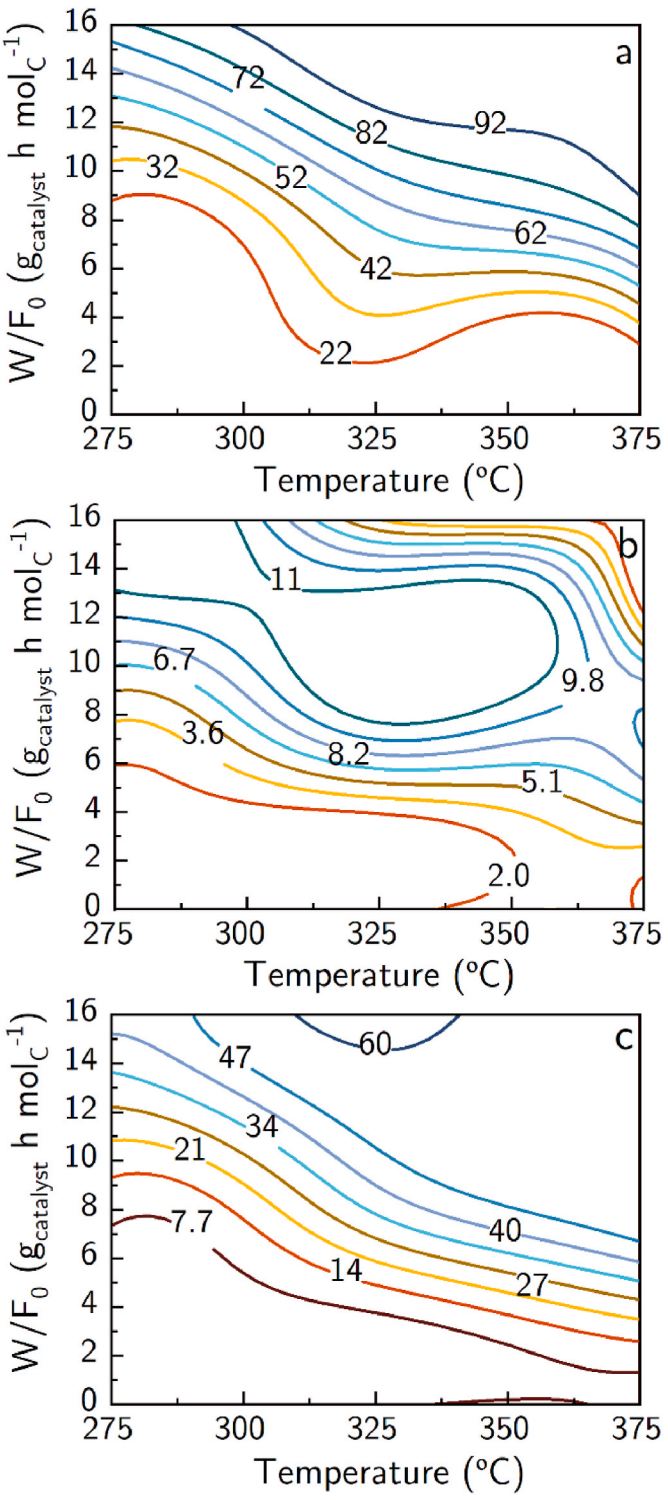

Fig. 9. Temperature-space time contour maps (in %) of: a) ethylene conversion, b) $C_4^=$ yield and c) C_{5+} yield. Reaction conditions: 1.5 bar; 3 h on stream.

3.4. Coke content and types in the catalyst

3.4.1. Effect of temperature

Fig. 10 shows the effect of reaction temperature on the TPS-N_2 (graph a) and TPO (b) profiles of the spent catalysts after 5 h on stream (pseudo-steady state). The amount of soft coke and hard coke (types I and II) have been calculated from the N_2-TPS and gaussian deconvolution of the TPO profiles, respectively, and their corresponding values are summarized in Table 1.

Reaction temperature has a strong influence on the amount of soft coke (Fig. 10a), which is mainly composed of bulkier oligomers retained within the catalyst matrix [62,63]. As shown in Table 1 the content of this type of coke in the catalyst is high at 275 °C (2.7 wt%) and 300 °C (1.5 wt%) while it substantially decreases at higher temperature, being almost negligible at 375 °C. This trend of the soft coke content and its low value at high temperature can be explained by the fact that after reaction the catalyst bed is swept with a N_2 stream at the reaction temperature and pressure, which enables the removal of retained and physically adsorbed compounds (mainly in the matrix). These compounds (in this case oligomers) cannot be considered responsible for the coke formation because they will also be displaced to the exterior of the catalyst particle by the flow of reactant and products.

According to the hard coke characterization methodology, in the TPO profiles of the spent HZSM-5 catalysts (Fig. 10b) two types of hard coke can be distinguished, with a better definition of both peaks for the runs performed at 350 and 375 °C. Based on the literature on acid catalyst deactivation, these two types of coke are defined as [38,42,64]: coke type I, characterized by its low oxidation temperature (with a maximum at ~460 °C), is associated with less evolved coke with high H/C ratio; and, coke type II, characterized by high oxidation temperature (peak at ~550 °C) is related to coke with low H/C ratio. In the oligomerization of 1-butene on an agglomerated HZSM-5 zeolite catalyst, the presence of these two peaks was explained by Díaz et al. [38] by their different location in the catalyst particle. Hence, hard coke type I is deposited in the matrix (mesoporous structure), which facilitates its combustion at lower temperatures, whereas hard coke type II is deposited in the micropores of the zeolite, and, therefore, its combustion takes place at higher temperatures because of the constraints imposed by shape selectivity. This limitation of the combustion of coke occluded in the micropores has also been observed in the literature for other catalytic reactions [42,43,64].

Table 1
Effect of reaction temperature on the content of total coke (C_c), soft coke and types I and II of hard coke, and on the oxidation temperatures of the different types of coke (T_I and T_{II}). The results correspond to the $N_{2-\ TPS}$and TPO profiles plotted in Fig. 10.

T (°C)	C_C (wt %)	Soft coke	Hard coke			
		Content (wt %)	Coke I (wt %)	T_I (°C)	Coke II (wt %)	T_{II} (°C)
275	4.8	2.7	1.6	449	0.5	543
300	4.3	1.5	2.3	470	0.6	547
325	5.0	0.4	3.1	478	1.5	556
350	5.5	0.1	2.8	465	2.6	557
375	4.4	0.08	3.2	473	1.2	568

The reaction temperature has a relevant incidence on the content and nature of the hard coke, which is attributable to its effect on: i) product distribution, by the different incidence of temperature in the reactions taking place in the oligomerization mechanism (Fig. 1), and based on the different role as coke precursors of the different compounds, and: ii) the reactions involved in the formation of hard coke from these precursors [63]. Table 1 shows the different contents of the two types of hard coke and the temperatures corresponding to their maximum burning rate, T_I and T_{II}. It is observed that higher reaction temperature gives way to an increase in the overall hard coke content, from 2.1 wt% at 275 °C up to 5.4 wt% at 350 °C, which decreases to 4.3 wt% at 375 °C. High hard coke content has also been reported in the literature in the oligomerization of ethylene [22], propylene [23,65] and butene [38]. Halmenschlager et al. [23] highlight the importance of the catalyst shape selectivity on the hard coke content, due to the different ease for the extent of

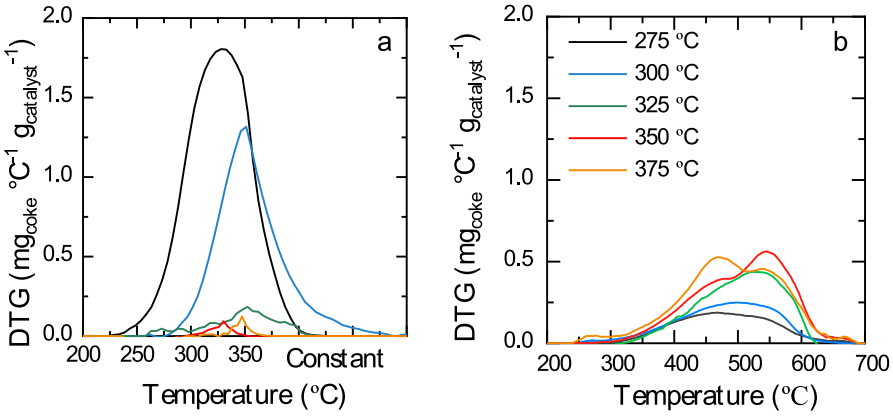

Fig. 10. Effect of reaction temperature on the (a) TPS-N_2 and (b) TPO profiles of the spent catalysts. Reaction conditions: 1.5 bar; space time, 10.6 $g_{catalyst}$ h mol_C^{-1}; 5 h on stream.

condensation and hydrogen transfer reactions involved in its formation.

Furthermore, at higher reaction temperature, as observed in Table 1, the content of the two types of hard coke increases up to 325 °C, changing the trend at 375 °C for both. This maximum of the hard coke content at 325 °C is more pronounced for type II, which decreases to 1.2 wt% at 375 °C. These results are consistent with the established effect of the temperature on the mechanism of coke formation from hydrocarbons over acid catalyst [42,63,64]. Thus, an increase in the reaction temperature favors the extent of the condensation and hydrogen transfer reactions, with olefinic oligomers as coke precursors. According to the results in Table 1, the evolution of the hard coke type II is clearly slowed down at 375 °C. The explanation lies on the lower adsorption rate in the acid sites and on the higher diffusivity of the oligomers, which is effective at this temperature as a counterpart to the increased rate of their condensation reactions to coke. The partial cracking of the coke precursors may also contribute to the lower deposition of hard coke at 375 °C. This temperature dependent activity of HZSM-5 zeolite is well established [42,43,64]. Moreover, at 375 °C, as a consequence of hydrogen transfer reactions, the concentration of paraffins is high, which are less active than olefins in coke formation reactions [66].

However, a raise in reaction temperature up to 375 °C is effective for increasing the extent of secondary coke condensation reactions inside the zeolite crystalline channels, and consequently, the combustion temperature peak of hard coke type II (T_{II} in Table 1) increases progressively in the studied range of reaction temperature, up to 568 °C, which corresponds to a developed coke [38,43]. Moreover, the results in Table 1 also highlight the positive effect of the catalyst matrix, by retaining substantial fractions of the overall coke (soft coke and hard coke type I), which explains the reduced content of hard coke type II in the zeolite micropores up to 325 °C. The high coke content confined in the matrix (hard coke type I) at 375 °C (3.2 wt%) justifies the favorable effect of a temperature raise on the oligomerization reactions.

In Fig. 11 the TEM images of the catalysts used at reaction runs carried out at 275 °C and 350 °C are depicted. The TEM images allow to distinguish in Fig. 11a the coke type I deposited on the matrix. On the other hand, coke type II deposited in the zeolite contributes to the intensity of the TEM images in Fig. 11b. The TEM images confirm in a qualitative way the results gathered in Table 1 on coke content. Thus, comparing Fig. 11b, corresponding to a reaction run (5 h) carried out at 350 °C, with Fig. 11a of a reaction carried out at 275 °C, the intensity of the former confirms the greater content of hard coke of the sample obtained at 350 °C (5.4% vs 2.1% obtained at 275 °C).

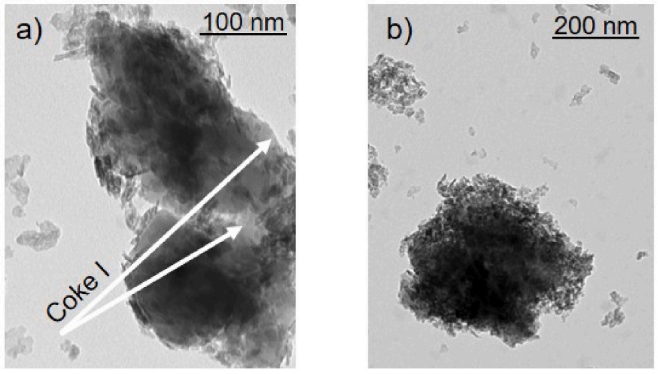

Fig. 11. TEM images of catalysts used in 5 h runs at: a) 275 °C and b) 350 °C.

3.4.2. *Effect of space time*

Fig. 12 shows the effect of space time at 325 °C on the N_2-TPS (graph a) and TPO (b) profiles of the spent catalyst. It is noteworthy that the effect of space time on the amount and types of coke is less significant than of reaction temperature (Section 3.4.2). This greater effect of the temperature on the soft coke (physically retained oligomers) is explained by the lower adsorption of the oligomers with increasing temperature as explained above. The lower content of soft coke on the catalyst with increasing contact time (from 1.1 wt% for 2.7 $g_{catalyst}$ h mol_C^{-1} to 0.4 wt% for 16.2 $g_{catalyst}$ h mol_C^{-1}) can be explained by the evolution of the oligomers towards higher molecular weight compounds, requiring higher temperature for their desorption from the catalyst (Fig. 12a). The smaller effect of space time on hard coke deposition compared to the effect of reaction temperature is explained by the fact that temperature affects the kinetic parameters of the reactions for coke formation and its evolution, as well as the diffusivity of coke precursors. The effect of the increase in space time is related to the greater extent of the reactions involved in oligomerization (Fig. 1), and the consequent change in the concentration of all the components. Thus, total hard coke content (responsible for deactivation) slightly increases from 4.3 wt% up to 5.2 wt% with increasing space time, although the evolution of hard coke type I in the matrix and type II in the zeolite micropores can be distinguished. Hence, the content of type I increases with increasing space time as a consequence of the greater extent of its formation reactions (condensation and hydrogen transfer) with increasing contact time. This trend is not observed with the hard coke type II, where the maximum content (2.7 wt%) for an intermediate space time value of 5.4 $g_{catalyst}$ h mol_C^{-1} can be attributed to the partial oligomer cracking (coke precursors) above this space time. This cracking is not observed in the evolution of hard coke type I because the catalyst matrix (γ-Al_2O_3 and α-Al_2O_3) has no cracking activity. Furthermore, as observed in Fig. 12b, the space time does not show a defined effect on the condensation of hard coke type II, whose maximum combustion rate is located within the 540–560 °C range.

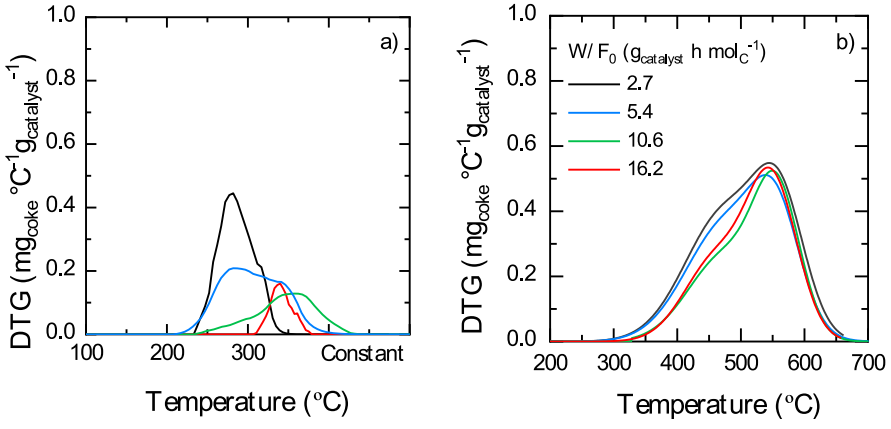

Fig. 12. Effect of space time (W/F_0) on the (a) N_2-TPS and (b) TPO profiles of the spent catalysts. Reaction conditions: 1.5 bar; 325 °C; 5 h on stream.

4. Conclusions

The oligomerization of ethylene at slightly over atmospheric pressure (1.5 bar) on a catalyst with hierarchical structure prepared by agglomeration of a HZSM-5 zeolite (SiO_2/Al_2O_3 of 30) in a mesoporous matrix of γ-Al_2O_3 and α-Al_2O_3, is an attractive process to obtain high yield of liquid fuels. The presence of the matrix is effective for the catalyst to maintain a pseudo-steady state of relevant remnant activity since a significant fraction of coke is retained in the matrix mesopores.

Temperature (to a greater extent) and space time have a relevant effect on ethylene conversion and product distribution by influencing the extent of oligomerization, cracking, hydrogen transfer and coke formation reactions. 325 °C is a suitable temperature to maximize the yield of C_{5+} liquid fuels (85.5 vol%) with a gasoline yield (distilling in the 50–150 °C range) of 60%, for a value of space time, above 10.6 $g_{catalyst}$ h mol_C^{-1}. The gasoline obtained under these conditions is mostly olefinic (49%), whereas a higher temperature and space time gives way to higher content of aromatics and paraffins within the gasoline, which are formed by condensation and hydrogen transfer reactions, respectively. This composition and the absence of sulfur and nitrogen are interesting for the incorporation of this gasoline into the refinery gasoline pool, because they facilitate the hydrogenation and reforming treatments required for the production of commercial gasoline.

The results of coke analysis of the spent catalysts evidence that the coke fractions deposited in the matrix and in the crystalline channels of the zeolite will contribute to catalyst deactivation. Furthermore, it has been proven that reaction temperature has a significant impact on coke content and distribution. Thus, above 325 °C, the increase in the cracking rate of the hard coke precursors in the interior of the zeolite micropores results in a decrease in the content of this coke fraction. In addition, the slight increase of hard coke in the catalyst particle with increasing space time, coinciding with the increase in aromatic fraction, allows identifying these compounds as intermediates in the formation of hard coke.

The results show the potential of this process, without compression costs, to valorize secondary gaseous olefinic streams in refinery processes. Furthermore, the integration of this process with those for the sustainable production of olefins from biomass (as methanol, ethanol and bio-oil), wastes or CO_2, can provide liquid fuels free of sulfur and nitrogen compounds.

Credit author statement

Zuria Tabernilla: Conceptualization, Methodology, Investigation, Data curation, Writing- Original Draft, Writing- Review & Editing, Ainara Ateka: Validation, Visualization, Writing- Original Draft, Writing- Review & Editing, Javier Bilbao: Conceptualization, Data curation, Writing- Original Draft, Writing- Review & Editing, Project administration, Funding acquisition, Andrés T. Aguayo: Methodology, Resources, Supervision, Project administration, Funding acquisition, Eva Epelde: Conceptualization, Data curation, Writing- Original Draft, Writing- Review & Editing.

Declaration of competing interest

The authors declare that they have no known competing financial interests or personal relationships that could have appeared to influence the work reported in this paper.

Data availability

The authors are unable or have chosen not to specify which data has been used.

Acknowledgments

This work has been carried out with the financial support of the Ministry of Economy and Competitiveness of the Spanish Government (Project PID2022-140584OB-I00); the Basque Government (Project IT1645-22); and the European Regional Development Funds (ERDF) and the European Commission (HORIZON H2020-MSCA RISE 2018. Contract No. 823745). Z. Tabernilla is grateful for the PhD grant from the Department of Education, University and Research of the Basque Government (PRE_2022_2_0136). The authors thank for technical and human support provided by SGIker (UPV/EHU).

Nomenclature

Abbreviations

ASF	Anderson-Schulz-Flory distribution
BAS	Brönsted Acid Sites
CN	Carbon number
DCU	Delayed Coking Unit
DME	Dimethyl ether
DTG	Derivative Thermogravimetry
DTO	Dimethyl ether to olefins
FCC	Fluid Catalytic Cracking
HT	High Desorption Temperature
LAOs	Linear alpha olefins
LAS	Lewis Acid Sites
LT	Low Desorption Temperature
MOGD	Mobil Olefins to Gasoline and Distillate
MTO	Methanol to Olefins
SHOP	Shell's Higher Olefins Process
TPD	Temperature Programmed Desorption
N_2-TPS	Temperature Programmed Sweeping with N_2
TPO	Temperature Programmed Oxidation

Variables

F_0, F	Ethylene molar flow rate in the feed an in the oulet stream, mmolC min-1
F_i	Molar flow rate of i lump in the product stream, mmolC min-1
P	Pressure, bar
S_i	Product selectivity, %
T	Temperature, °C
W/F_0	Space time, g h molC-1
X	Ethylene conversion, %
Y_i	Product yield, %

Appendix A. Supplementary data

Supplementary data to this article can be found online at https://doi.org/10.1016/j.energy.2023.128703.

References

[1] Liu C, Liu S, Zhou H, Su J, Jiao W, Zhang L, et al. Selective conversion of syngas to aromatics over metal oxide/HZSM-5 catalyst by matching the activity between CO hydrogenation and aromatization. Appl Catal A Gen 2019;585:117206. https://doi.org/10.1016/j.apcata.2019.117206.

[2] Díaz M, Epelde E, Tabernilla Z, Ateka A, Aguayo AT, Bilbao J. Operating conditions to maximize clean liquid fuels yield by oligomerization of 1-butene on HZSM-5 zeolite catalysts. Energy 2020;207:118317. https://doi.org/10.1016/j.energy.2020.118317.

[3] Gao R, Zhang L, Wang L, Zhang C, Jun KW, Kim SK, Park HG, Gao Y, Zhu Y, Wan H, Guan G, Zhao T. Efficient production of renewable hydrocarbon fuels using waste CO_2 and green H_2 by integrating Fe-based Fischer-Tropsch synthesis and olefin oligomerization. Energy 2022;248:123616. https://doi.org/10.1016/j.energy.2022.123616.

[4] Quann RJ, Green LA, Tabak SA, Krambeck FJ. Chemistry of olefin oligomerization over zsm-5 catalyst. Ind Eng Chem Res 1988;27:565–70. https://doi.org/10.1021/ie00076a006.

[5] Tian P, Wei Y, Ye M, Liu Z. Methanol to olefins (MTO): from fundamentals to commercialization. ACS Catal 2015;5:1922. https://doi.org/10.1021/acscatal.5b00007. –38.

[6] Cordero-Lanzac T, Aguayo AT, Bilbao J. Reactor-regenerator system for the dimethyl ether-to-olefins process over HZSM-5 catalysts: conceptual development and analysis of the process variables. Ind Eng Chem Res 2020;59:14689–702. https://doi.org/10.1021/acs.iecr.0c02276.

[7] Kamkeng ADN, Wang M, Hu J, Du W, Qian F. Transformation technologies for CO_2 utilisation: current status, challenges and future prospects. Chem Eng J 2021;409:128138. https://doi.org/10.1016/j.cej.2020.128138.

[8] Ateka A, Rodriguez-Vega P, Ereña J, Aguayo AT, Bilbao J. A review on the valorization of CO_2. Focusing on the thermodynamics and catalyst design studies of the direct synthesis of dimethyl ether. Fuel Process Technol 2022;233:107310. https://doi.org/10.1016/j.fuproc.2022.107310.

[9] Pawelec B, Guil-López R, Mota N, Fierro J, Navarro Yerga R. Catalysts for the conversion of CO_2 to low molecular weight olefins—a review. Materials 2021;14:6952. https://doi.org/10.3390/ma14226952.

[10] Portillo A, Ateka A, Ereña J, Bilbao J, Aguayo AT. Alternative acid catalysts for the stable and selective direct conversion of CO_2/CO mixtures into light olefins. Fuel Process Technol 2022;238:107513. https://doi.org/10.1016/j.fuproc.2022.107513.

[11] Freitas ER, Gum CR. Shell's higher olefins process. Chem Eng Prog 1979;75:73–769.

[12] Speiser F, Braunstein P, Saussine L. Catalytic ethylene dimerization and oligomerization: recent developments with nickel complexes containing P,N-chelating ligands. Acc Chem Res 2005;38:784–93. https://doi.org/10.1021/ar050040d.

[13] McGuinness DS. Olefin oligomerization via metallacycles: dimerization, trimerization, tetramerization, and beyond. Chem Rev 2011;111:2321–41. https://doi.org/10.1021/cr100217q.

[14] Nicholas CP. Applications of light olefin oligomerization to the production of fuels and chemicals. Appl Catal A Gen 2017;543:82–97. https://doi.org/10.1016/j.apcata.2017.06.011.

[15] Zhang H, Li X, Zhang Y, Lin S, Li G, Chen L, Fang Y, Xin H, Li X. Ethylene oligomerization over heterogeneous catalysts. Energy Environ Focus 2014;3:246–56. https://doi.org/10.1166/eef.2014.1107.

[16] Ghashghaee M. Heterogeneous catalysts for gas-phase conversion of ethylene to higher olefins. Rev Chem Eng 2018;34:595–655. https://doi.org/10.1515/revce-2017-0003.

[17] Moussa S, Concepción P, Arribas MA, Martínez A. Nature of active nickel sites and initiation mechanism for ethylene oligomerization on heterogeneous Ni-Beta catalysts. ACS Catal 2018;8:3903–12. https://doi.org/10.1021/acscatal.7b03970.

[18] Moon S, Chae HJ, Park MB. Oligomerization of light olefins over ZSM-5 and beta zeolite catalysts by modifying textural properties. Appl Catal A Gen 2018;553:15–23. https://doi.org/10.1016/j.apcata.2018.01.015.

[19] Jin F, Yan Y, Wu G. Ethylene oligomerization over H- and Ni-form aluminosilicate composite with ZSM-5 and MCM-41 structure: effect of acidity strength, nickel site and porosity. Catal Today 2019;355:148–61. https://doi.org/10.1016/j.cattod.2019.06.050.

[20] Koninckx E, Mendes PSF, Thybaut JW, Broadbelt LJ. Ethylene oligomerization on nickel catalysts on a solid acid support: from New mechanistic insights to tunable bifunctionality. Appl Catal A Gen 2021;624:118296. https://doi.org/10.1016/j.apcata.2021.118296.

[21] Koninckx E, Gounder R, Thybaut JW, Broadbelt LJ. Kinetic modeling of ethene oligomerization on Bifunctional nickel and acid β zeolites. Ind Eng Chem Res 2022;61:3860–76. https://doi.org/10.1021/acs.iecr.1c04105.

[22] Andrei RD, Borodina E, Minoux D, Nesterenko N, Dath J-P, Cammarano C. Hulea V. Ethylene oligomerization from diluted stream over Ni-containing heterogeneous catalysts. Ind Eng Chem Res 2020;59:1746–52. https://doi.org/10.1021/acs.iecr.9b05576.

[23] Halmenschlager CM, Brar M, Apan IT, de Klerk A. Oligomerization of fischer–tropsch tail gas over H-ZSM-5. Ind Eng Chem Res 2016;55:13020–31. https://doi.org/10.1021/acs.iecr.6b03861.

[24] Cordero-Lanzac T, Aguayo AT, Gayubo AG, Bilbao J. Consideration of the activity distribution using the population balance theory for designing a dual fluidized bed reactor-regenerator system. Application to the MTO process. Chem Eng J 2021;405:126448. https://doi.org/10.1016/j.cej.2020.126448.

[25] Gayubo AG, Alonso A, Valle B, Aguayo AT, Bilbao J. Selective production of olefins from bioethanol on HZSM-5 zeolite catalysts treated with NaOH. Appl Catal B Environ 2010;97:299–306. https://doi.org/10.1016/j.apcatb.2010.04.021.

[26] Gayubo AG, Valle B, Aguayo AT, Olazar M, Bilbao J. Olefin production by catalytic transformation of crude bio-oil in a two-step process. Ind Eng Chem Res 2010;49:123–31. https://doi.org/10.1021/ie901204n.

[27] Artetxe M, Lopez G, Elordi G, Amutio M, Bilbao J, Olazar M. Production of light olefins from polyethylene in a two-step process: pyrolysis in a conical spouted bed and downstream high-temperature thermal cracking. Ind Eng Chem Res 2012;51:13915–23. https://doi.org/10.1021/ie300178e.

[28] Valle B, Alonso A, Atutxa A, Gayubo AG, Bilbao J. Effect of nickel incorporation on the acidity and stability of HZSM-5 zeolite in the MTO process. Catal Today 2005;106:118–22. https://doi.org/10.1016/j.cattod.2005.07.132.

[29] Garwood WE. Conversion of C 2 -C 10 to Higher olefins over synthetic zeolite ZSM-5. ACS Symp Ser 1983;23:383–96. https://doi.org/10.1021/bk-1983-0218.ch023.

[30] Berta AH, Hwang HD, Asfha HB, Kang NY, Kim K, Park YK. Reaction mechanism and kinetic modeling of olefin conversion over phosphorus modified ZSM-5 catalyst. Kor J Chem Eng 2022;39:1460–71. https://doi.org/10.1007/s11814-021-1016-9.

[31] Zhang J, Tang R, Shen Z, Liang S, Zhong H. Catalytic oligomerization of ethylene over nano-sized HZSM-5. J Energy Inst 2020;93:2550–7. https://doi.org/10.1016/j.joei.2020.09.002.

[32] Bickel EE, Gounder R. Hydrocarbon products occluded within zeolite micropores impose transport barriers that regulate brønsted acid-catalyzed propene oligomerization. JACS Au 2022;2:2585–95. https://doi.org/10.1021/jacsau.2c00462.

[33] Bickel EE, Lee S, Gounder R. Influence of brønsted acid-site density on reaction-diffusion phenomena that govern propene oligomerization rate and selectivity in MFI zeolites. ACS Catal 2023;13:1257–69. https://doi.org/10.1021/acscatal.2c05184.

[34] Jin F, Zhang P, Wu G. Fundamental kinetics model of acidity-activity relation for ethylene oligomerization and aromatization over ZSM-5 zeolites. Chem Eng Sci 2021;229:116144. https://doi.org/10.1016/j.ces.2020.116144.

[35] Arnold U, Betz M, Fuchs C, Zevaco TA, Sauer J. Production of hydrocarbon fuels by heterogeneously catalyzed oligomerization of ethylene: tuning of the product distribution. SSRN Electron J 2022;166. https://doi.org/10.2139/ssrn.4111602.

[36] Liao M, Ning X, Chen J, Zheng J, Li W, Li R. Mesoporous ZSM-5 catalysts for the synthesis of clean jet-fuels by 1-hexene oligomerization. Fuel 2021;304:121383. https://doi.org/10.1016/j.fuel.2021.121383.

[37] Díaz M, Epelde E, Aguayo AT, Bilbao J. Low-pressure oligomerization of 1-butene to liquid fuels on HZSM-5 zeolite catalysts: effect of operating conditions. J Ind Eng Chem 2020;87:234–41. https://doi.org/10.1016/j.jiec.2020.04.006.

[38] Díaz M, Epelde E, Valecillos J, Izaddoust S, Aguayo AT, Bilbao J. Coke deactivation and regeneration of HZSM-5 zeolite catalysts in the oligomerization of 1-butene. Appl Catal B Environ 2021;291:120076. https://doi.org/10.1016/j.apcatb.2021.120076.

[39] Pérez-Uriarte P, Gamero M, Ateka A, Díaz M, Aguayo AT, Bilbao J. Effect of the acidity of HZSM-5 zeolite and the binder in the DME transformation to olefins. Ind Eng Chem Res 2016;55:1513–21. https://doi.org/10.1021/acs.iecr.5b04477.

[40] Valecillos J, Tabernilla Z, Epelde E, Sastre E, Aguayo AT, Castaño P. Quenching the deactivation in the methanol-to-olefin reaction by using tandem fixed-beds of ZSM-5 and SAPO-18 catalysts. Ind Eng Chem Res 2020;59:13892–905. https://doi.org/10.1021/acs.iecr.0c01616.

[41] Díaz-Rey MR, Paris C, Martínez-Franco R, Moliner M, Martínez C, Corma A. Efficient oligomerization of pentene into liquid fuels on nanocrystalline beta zeolites. ACS Catal 2017;7:6170–8. https://doi.org/10.1021/acscatal.7b00817.

[42] Ibáñez M, Pérez-Uriarte P, Sánchez-Contador M, Cordero-Lanzac T, Aguayo AT, Bilbao J, Castaño P. Nature and location of carbonaceous species in a composite HZSM-5 zeolite catalyst during the conversion of dimethyl ether into light olefins. Catalysts 2017;7:254. https://doi.org/10.3390/catal7090254.

[43] Cordero-Lanzac T, Ateka A, Pérez-Uriarte P, Castaño P, Aguayo AT, Bilbao J. Insight into the deactivation and regeneration of HZSM-5 zeolite catalysts in the conversion of dimethyl ether to olefins. Ind Eng Chem Res 2018;57:13689–702. https://doi.org/10.1021/acs.iecr.8b03308.

[44] Trueba D, Palos R, Bilbao J, Arandes JM, Gutiérrez A. Product composition and coke deposition in the hydrocracking of polystyrene blended with vacuum gasoil. Fuel Process Technol 2021;224. https://doi.org/10.1016/j.fuproc.2021.107010.

[45] Silva AF, Fernandes A, Antunes MM, Ribeiro MF, Silva CM, Valente AA. Catalytic conversion of 1-butene over modified versions of commercial ZSM-5 to produce clean fuels and chemicals. ChemCatChem 2019;11:4196–209. https://doi.org/10.1002/cctc.201801975.

[46] Coelho A, Caeiro G, Lemos MANDA, Lemos F, Ribeiro FR. 1-Butene oligomerization over ZSM-5 zeolite: Part 1 - effect of reaction conditions. Fuel 2013;111:449–60. https://doi.org/10.1016/j.fuel.2013.03.066.

[47] Koninckx E, Mendes PSF, Thybaut JW, Broadbelt LJ. Ethylene oligomerization on nickel catalysts on a solid acid support: from New mechanistic insights to tunable bifunctionality. Appl Catal A Gen 2021;624:118296. https://doi.org/10.1016/j.apcata.2021.118296.

[48] Jan O, Song K, Dichiara A, Resende FLP. Ethylene oligomerization over Ni–Hβ heterogeneous catalysts. Ind Eng Chem Res 2018;57:10241–50. https://doi.org/10.1021/acs.iecr.8b01902.

[49] Fernandes DS, Veloso CO, Henriques CA. Ethylene conversion into propylene and aromatics on HZSM-5: insights on reaction routes and water influence. Catal Lett 2020;150:738–52. https://doi.org/10.1007/s10562-019-02954-w.

[50] Uslamin EA, Saito H, Kosinov N, Pidko E, Sekine Y, Hensen EJM. Aromatization of ethylene over zeolite-based catalysts. Catal Sci Technol 2020;10:2774–85. https://doi.org/10.1039/c9cy02108f.

[51] Sydora OL. Selective ethylene oligomerization. Organometallics 2019;38:997–1010. https://doi.org/10.1021/acs.organomet.8b00799.

[52] Moussa S, Arribas MA, Concepción P, Martínez A. Heterogeneous oligomerization of ethylene to liquids on bifunctional Ni-based catalysts: the influence of support properties on nickel speciation and catalytic performance. Catal Today 2016;277:78–88. https://doi.org/10.1016/j.cattod.2015.11.032.

[53] Kwon M-H, Yoon JS, Lee M, Hwang DW, Kim Y, Park MB, et al. One-post cascade ethylene oligomerization using Ni/Siral-30 and H-ZSM-5 catalysts. Appl Catal A Gen 2019;572:226–31. https://doi.org/10.1016/j.apcata.2018.12.005.

[54] Zhou H, Wang Y, Wei F, Wang D, Wang Z. Kinetics of the reactions of the light alkenes over SAPO-34. Appl Catal A Gen 2008;348:135–41. https://doi.org/10.1016/j.apcata.2008.06.033.

[55] Finiels A, Fajula F, Hulea V. Nickel-based solid catalysts for ethylene oligomerization-a review. Catal Sci Technol 2014;4:2412–26. https://doi.org/10.1039/c4cy00305e.

[56] Lavrenov AV, Karpova TR, Buluchevskii EA, Bogdanets EN. Heterogeneous oligomerization of light alkenes: 80 years in oil refining. Catalogue Index 2016;8:316–27. https://doi.org/10.1134/s2070050416040061.

[57] Lin B, Zhang Q, Wang Y. Catalytic conversion of ethylene to propylene and butenes over H-ZSM-5. Ind Eng Chem Res 2009;48:10788–95. https://doi.org/10.1021/ie901227p.
[58] Mehdad A, Lobo RF. Ethane and ethylene aromatization on zinc-containing zeolites. Catal Sci Technol 2017;7:3562–72. https://doi.org/10.1039/c7cy00890b.
[59] Yamazaki H, Yokoi T, Tatsumi T, Kondo JN. Ethene oligomerization on H-ZSM-5 in relation to ethoxy species. Catal Sci Technol 2014;4:4193–5. https://doi.org/10.1039/c4cy01028k.
[60] Cordero-Lanzac T, Aguayo AT, Castaño P, Bilbao J. Kinetics and reactor modeling of the conversion of: N -pentane using HZSM-5 catalysts with different Si/Al ratios. React Chem Eng 2019;4:1922–34. https://doi.org/10.1039/c9re00222g.
[61] Silva AF, Fernandes A, Antunes MM, Neves P, Rocha SM, Ribeiro MF, Pillinger M, Ribeiro J, Silva C, Valente A. TUD-1 type aluminosilicate acid catalysts for 1-butene oligomerisation. Fuel 2017;209:371–82. https://doi.org/10.1016/j.fuel.2017.08.017.
[62] Fan Y, Cai Y, Li X, Yin H, Xia J. Coking characteristics and deactivation mechanism of the HZSM-5 zeolite employed in the upgrading of biomass-derived vapors. J Ind Eng Chem 2017;46:139–49. https://doi.org/10.1016/j.jiec.2016.10.024.
[63] Guisnet M, Magnoux P. Organic chemistry of coke formation. Appl Catal A Gen 2001;212:83–96. https://doi.org/10.1016/S0926-860X(00)00845-0.
[64] Ibáñez M, Artetxe M, Lopez G, Elordi G, Bilbao J, Olazar M, et al. Identification of the coke deposited on an HZSM-5 zeolite catalyst during the sequenced pyrolysis-cracking of HDPE. Appl Catal B Environ 2014;148:436–45. https://doi.org/10.1016/j.apcatb.2013.11.023.
[65] Monama W, Mohiuddin E, Thangaraj B, Mdleleni MM, Key D. Oligomerization of lower olefins to fuel range hydrocarbons over texturally enhanced ZSM-5 catalyst. Catal Today 2020;342:167–77. https://doi.org/10.1016/j.cattod.2019.02.061.
[66] Cordero-Lanzac T, Martínez C, Aguayo AT, Castaño P, Bilbao J, Corma A. Activation of n-pentane while prolonging HZSM-5 catalyst lifetime during its combined reaction with methanol or dimethyl ether. Catal Today 2022;383:320–9. https://doi.org/10.1016/j.cattod.2020.09.015.